https://doi.org/10.48048/tis.2024.7370

Seismic Microzonation Map of Chiang Mai Basin, Thailand

Patinya Pornsopin[1,2], Passakorn Pananont[2,*], Kevin Patrick Furlong[3], Sophon Chaila[1], Chutimon Promsuk[1], Chirawat Kamjudpai[1] and Khomphet Phetkongsakul[1]

[1]Earthquake Observation Division, Thai meteorological Department, Bangkok 10260, Thailand
[2]Department of Earth Sciences, Faculty of Science, Kasetsart University, Bangkok 10900, Thailand
[3]Department of Geosciences, The Pennsylvania State University, Pennsylvania 16801, United States

([*]Corresponding author's e-mail: fscipkp@ku.ac.th)

Received: 11 August 2023, Revised: 13 September 2023, Accepted: 18 September 2023, Published: 10 January 2024

Abstract

The seismic site effect which is controlled by local geological conditions is a key parameter of seismic hazards analysis. This paper presents an observational study of microtremor data to investigate the dynamic characteristics of soil in the Chiang Mai basin (Chiang Mai and Lumphun province), Northern Thailand. The Chiang Mai basin was formed on terrace sediments and alluvium sediments. The horizontal vertical spectral ratio (HVSR) analyses of ambient noise data at 101 sites in the basin were analyzed for an average smoothed HVSR curve to estimate the amplification factor and fundamental resonance frequency of each observation point. We also evaluated the shear wave velocity using the HVSR inversion technique based on the diffuse field assumption. Tests undertaken include a comparison of the HVSR of a significant earthquake that was detected at stations in the basin and a nearby bedrock site. The results indicate that the resonance frequency ranges between 0.15 - 0.4 Hz at sites having large thicknesses of soft sediments. The lowest resonance frequencies occur in the center of the basin, whereas higher resonance frequencies were observed in the areas of the shallowest bedrock in the west and east of the basin. It can be inferred that the western margin of the Chiang Mai basin is a steep slope, while the eastern margin of the basin is a low-angle west-dipping basement. The amplification factor ranges between 3 - 5 times, in the middle of the basin. Most of the Chiang Mai basin area is classified as site D soil (stiff soil) relative to alluvium sediments, and a region of class C soil (very dense soil) conforms to the terrace sediments located on the eastern edge of the basin. The soil classification is based on shear wave velocity (Vs30) determined by HVSR inversion.

Keywords: Site effect, Amplification of ground motions, Fundamental frequency, Seismic microzonation, Chiang Mai basin, Thailand, HVSR inversion

Introduction

Chiang Mai, a major city in northern Thailand, is situated within a sedimentary basin (**Figure 1**). There have been small and moderate earthquakes reported in the Chiang Mai region over the past several years. In addition to earthquakes in Thailand, there are moderate and strong earthquakes nearby in Myanmar, which have been felt in Chiang Mai and have produced some damage.

The Chiang Mai basin is primarily affected by earthquakes in the Mae Tha Fault Zone (**Figure 1**), which also includes some hidden faults in the basin area [1]. The 2 main faults of the fault zone extend along the east and the west sides of the Chiang Mai Basin. The S-shaped fault system that bounds the basin to the east of Chiang Mai, includes the Nam Mae Lai fault segment which is a normal fault. The Doi-Sa-Ket fault segment located to the west is a right-lateral strike-slip fault and the Mae Tha fault further south is a left-lateral strike-slip fault segment. On the western edge of the basin, there are 2 fault segments, the Mae Rim Fault, which is a normal fault, and the Mae Wang Fault segment, which is a left-lateral strike-slip fault (**Figure 1**).

The seismicity of Chiang Mai and surrounding regions during the period 1922 - 2023, reported by the Thai Meteorological Department (TMD), shows earthquakes occur mostly at shallow depths within the basin (**Figure 1**). Most earthquakes that have occurred in the Chiang Mai basin have a magnitude of less than 3.0. The largest earthquake to occur in this area is magnitude 5.1 ML, which occurred in the Mae Rim district (red star in **Figure 1**), 16 kilometers away from the city of Chiang Mai on 13 December 2006. It caused severe damage throughout the Chiang Mai basin.

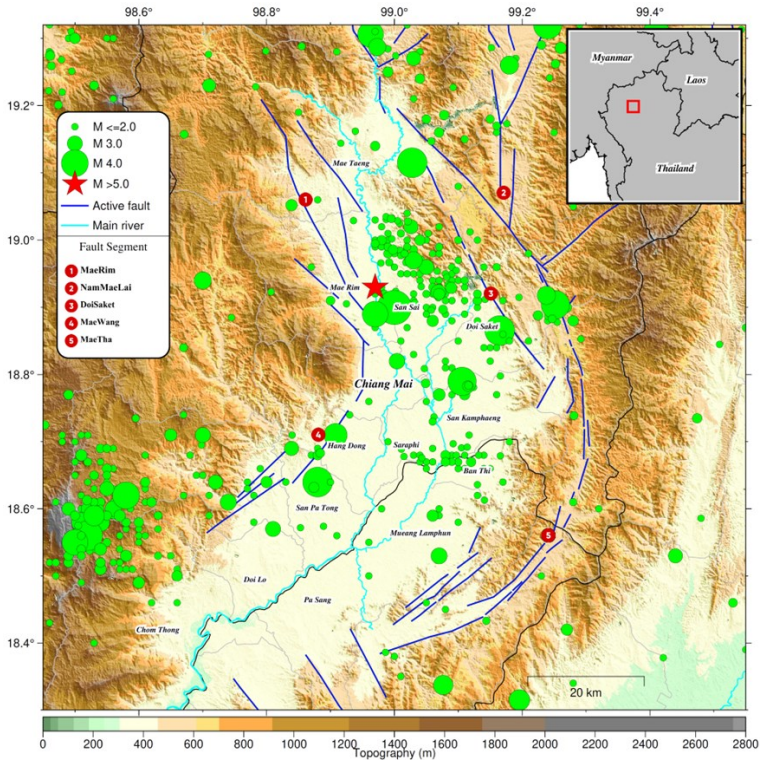

Figure 1 Seismicity in Chiang Mai basin and surrounding areas during 1922 - 2023. The faults shown are active faults provided by the Department of Mineral Resources (DMR). The seismicity data are reported by the Thai Meteorological Department (TMD).

The North-South trending Chiang Mai basin is the largest Cenozoic rift basin in northern Thailand [2], within the Chiang Mai and Lamphun provinces. Geologic mapping [3] indicates that it is filled by tertiary and quaternary (Qt) and alluvium (Qa) sediments bounded by mountain ridges as shown in **Figure 2**. These unconsolidated sediments were deposited relatively recently by streams or other bodies of running water, potentially associated with the Ping River and Kuang River that flow through the Chiang Mai and Lamphun area from north to south. Gravity and seismic studies indicate that Cenozoic sediments in the Chiang Mai basin are up to 2.5 km thick [4]. A vertical electrical sounding survey conducted by Mankhemthong *et al.* [5] in the eastern Chiang Mai basin shows that the sediment layer thickens westward into the central Chiang Mai basin, increasing from 17 m in the east to greater than 500 m in the basin center. The NEHRP site classification map of Chiang Mai City determined from the multichannel analysis of surface waves (MASW) method found that Chiang Mai City is mostly situated on Class D soil (249 - 360 m/s) [6]. Regions on the west side of the Ping River have higher Vs30 than on the east side of the river. Thitimakorn and Raenak [7] performed studies of MASW in Lumphun City, with the results showing that the Lumphun City area is located on class D soil (east, north, and west parts) and class C soil in the central and southern parts; with soil amplification between 1.4 to 2.8. Thamarux *et al.* [8] studied the soil classification in the Chiang Mai, Chiang Rai, and Lamphun regions based on geomorphology and the Vs30 determined from the spatial autocorrelation (SPAC) method. Their results show that most of the Chiang Mai basin has NEHRP class D soil with the edge of the basin class C. Poovarodom *et al.* [9] determined the Vs30 to be less than 290 m/s in the middle of the Chiang Mai basin, from an inversion using the Centerless Circular Array method [10].

Site effects are a common cause of seismic ground motion amplification at the fundamental frequency of the unconsolidated sediments. This can increase the damage from an earthquake and is very important in regions containing a thick layer of unconsolidated sediments, such as in the Chiang Mai basin. This research is focused on determining the seismic microzonation of the Chiang Mai basin area to investigate the dynamic characteristics of soil in order to assess the potential effects of earthquake shaking. We use microtremor measurements at 101 survey points covering the Chiang Mai and Lumphun provinces using the horizontal vertical spectral ratio (HVSR) technique [11]. This is a well-used investigation tool for seismic microzonation and earthquake site characterization, convenient to implement and cost-effective. In the previous 5 years, HVSR surveys were widely used to study the subsurface structure of different areas

(e.g., [12-19]). The utilization of this technique also be used to obtain other subsurface features, such as for groundwater surveys [20, 21].

The results of this study provide amplification and fundamental frequency maps, which were compared to earthquake HVSR of large earthquakes recorded by seismic stations in the Chiang Mai basin and on a rock site close to the basin. The maps of average shear wave velocity in the upper 30 m is determined through an inversion of HVSR, which is used to classify soil types according to the National Earthquake Hazard Reduction Program (NEHRP) [22] classification, for seismic hazard planning in terms of mitigation and response in Chiang Mai basin.

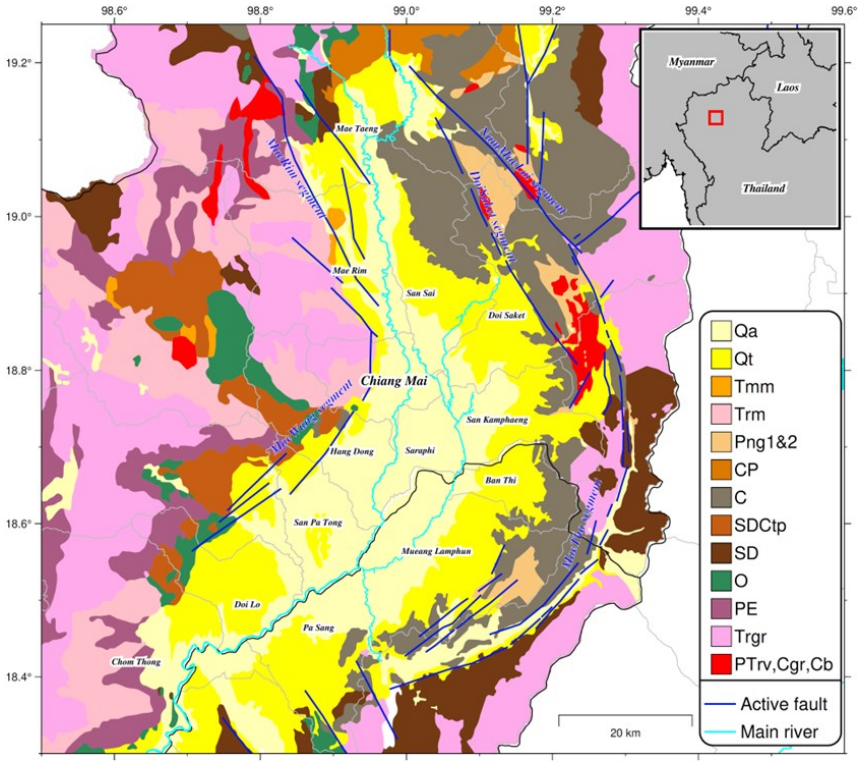

Figure 2 Geologic map of the Chiang Mai basin and surrounding area including the Mae The active fault zone [3].

Materials and methods

Microtremor measurements

We used a SARA SL-06 24 bit A/D datalogger connected to a SS-05 tri-axial velocity seismometer with a natural frequency of 0.5 Hz (2 s) and sensitivity of 400 V/m/s, this sensor is appropriate for the HVSR survey because its sensors have high stability, robustness and can withstand tilting.

Most (60 %) of the survey points are in temples, appropriate for this analysis because they are built on old soil that has not been reclaimed and are generally in quiet areas. We particularly selected sites on temple grounds near the base of the old ordination hall or pagoda. An example of a field survey site is shown in **Figure 3(a)**. Other survey points were located at government offices, schools, and public parks. The sensors were placed far away from any transient noise sources on soil, a concrete base, or a precast concrete slab, which is well coupled to the underlying ground. We covered the sensor with a plastic case to prevent effects from sunlight and wind. The distance between survey points in the Chiang Mai central city

is approximately 1 - 2 km and in other areas in the basin of about 5 - 6 km on average. The duration of data collection at each survey point is approximately 1 - 3 h, depending on the time and place.

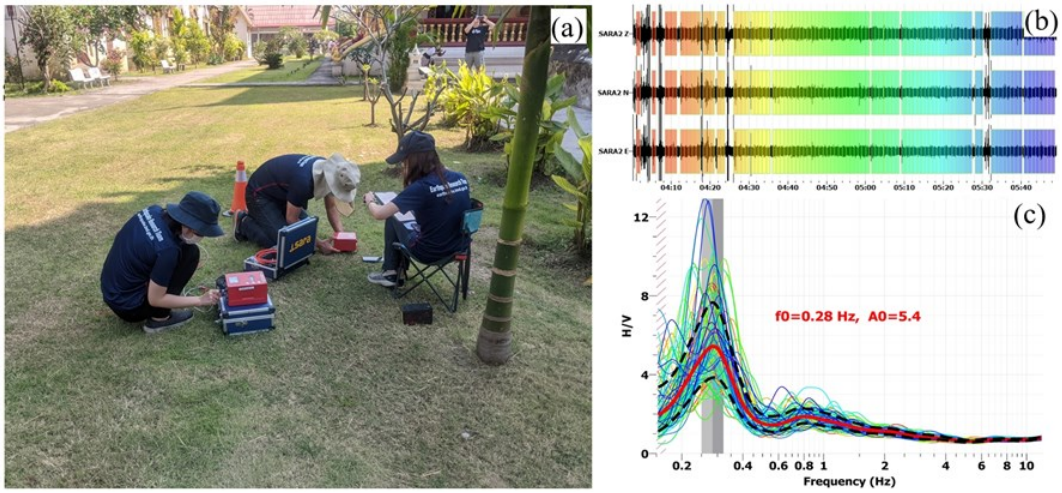

Figure 3 (a) Field installation of equipment at survey point 15, which is placed near the old pagoda base in the area of Wat Chiang Man temple in downtown Chiang Mai. (b) Raw waveform data triggered by the STA/LTA ratio for each 60-s window segment, which also shows the transient signals that have been eliminated, and (c) The HVSR curve for each segment and average (red curve), which indicates the fundamental frequency at 0.28 Hz and an HVSR amplification of 5.4.

HVSR analysis

The HVSR method allows us to obtain subsurface information from single station measurements [11] and consists of estimating the ratio between the Fourier amplitude spectra of the horizontal (H) to vertical (V) components for several time windows of ambient noise recorded to produce a smoothed HVSR curve. Taking an average over all windows, these curves represent the amplification factor and predominant frequencies.

We use Geopsy software (www.geopsy.org) for the HVSR analysis. The data were divided into non-overlapping 60-s windows to encompass the expected fundamental frequency, prevent repetition, and guarantee that each window contains unique information. Each window was tapered with a Hamming window and using the ratio of short-term average (STA) and long-term average (LTA) of 1 and 90 s, with minimum and maximum ratios of 0.2 and 2.3, respectively, to reject transient signals. The individual HVSR spectra were smoothed using a Konno-Ohmachi smoothing function [23] with a smoothing coefficient of 50 %. The horizontal component spectra have been computed by averaging E-W and N-S components using a squared average. An example HVSR analysis for survey point 15 is shown in **Figures 3(b) - 3(c)**, using 92 window segments selected for the average HVSR curve, which indicates the fundamental frequency of 0.28 Hz and an HVSR amplification of 5.4. In this analysis, a reliable HVSR curve and clear HVSR peaks for the fundamental frequency of mean HVSR curves will be considered as a quality criteria according to the recommendations in the SESAME guideline [24].

In the case of multiple peaks of the HVSR curve, we check each peak with the random decrement technique [25] to measure the damping of signals around the narrow frequency range of interest to identify industrial vibration sources (machines, water pumps, buildings, trees, etc.). Very low damping ratios of 1

% or less indicate that these HVSR peaks originate from anthropogenic sources, which we do not use in the interpretation or the HVSR inversion. An example of multiple peaks case is shown in **Figure 4**.

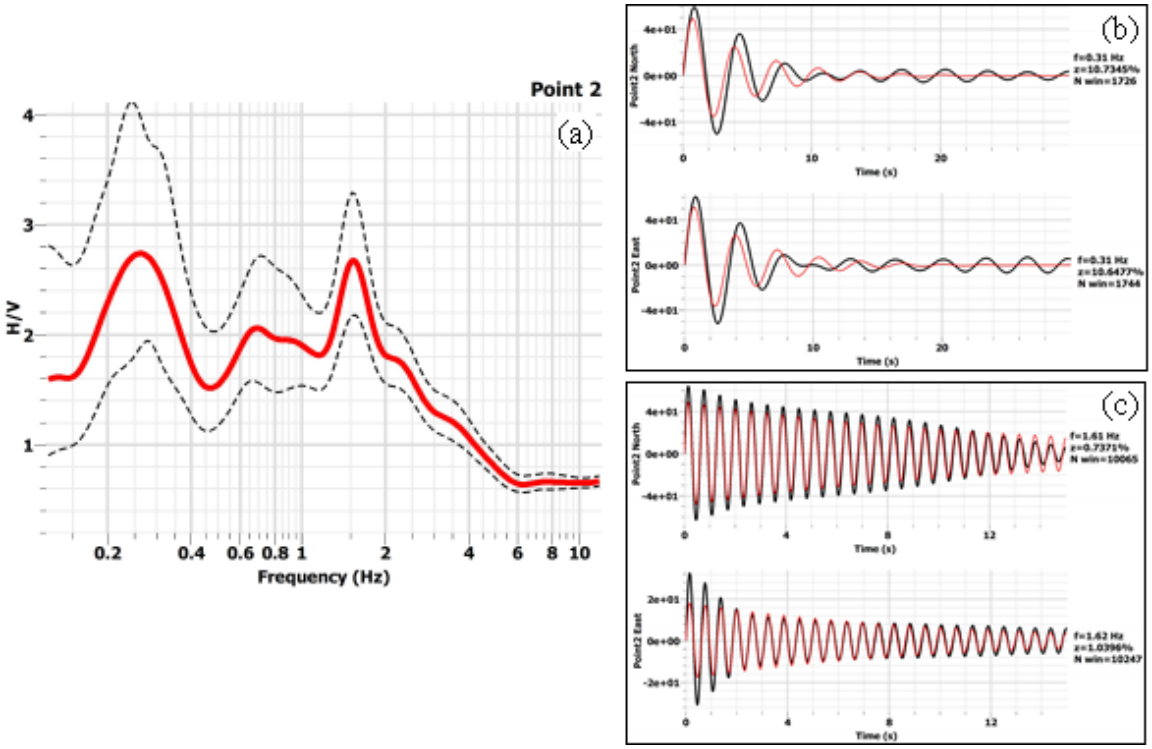

Figure 4 Assessing multiple peak HVSR results for human or natural sources by random decrement technique to estimate damping of horizontal component signals recorded (survey Point 2). (a) The HVSR curve shows 2 peaks at frequencies ~0.27 and ~1.6 Hz. (b) Horizontal component data filtered between 0.17 and 0.4 Hz; the average damping ratio of the fitted curve is ~10.7 %. The black solid line is the average curve with the red line being the fit to the curve by an exponentially decreasing sine function. (c) Horizontal component data filtered between 1.3 and 1.9 Hz; the average damping ratio of the fitted curve is ~0.8 %.

HVSR inversion

For the HVSR method, an inversion technique is used to estimate the value of the shear wave velocity, density, and Poisson's ratio of the subsurface [26]. We used TerraWare-HV code (https://github.com/sainosmichelle/TerraWare-HV) in the HVSR inversion process to compute the inversion of the HVSR curve for shear wave velocity profiles based on the diffuse field assumption. The HVSR curve as a function of the angular frequency (ω) can be represented as the energy density of the diffuse field, which is directly related to the imaginary component of Green's functions (G_{11}, G_{22}, G_{33}) at the source (x) according to the formulation [26,27];

$$[HVSR](\omega) = \sqrt{\frac{Im[G_{11}(x,x;\omega)]+Im[G_{22}(x,x;\omega)]}{Im[G_{33}(x,x;\omega)]}}$$

The components of the Green's function are related to geometry and material properties of the layered media in terms of P and S wave velocity, densities, and thickness. The inversion of HVSR curve is solved by adjusting geometry and material properties to satisfy data observations. This approach can be found in other studies, such as García-JerezandPiña-Flores [27] and Sánchez-Sesma *et al.* [28], with application to Ischia Island (Italy) [29] and Bengal Basin (Bangladesh) [30].

We assumed a 16-layer starting model where the layer thickness varied (**Table 1**) depending on the fundamental frequency (f_0) of the HVSR curve, which is estimated from the shear wave velocity in the Chiang Mai basin obtained in previous studies [5]. The thickness (h) is the relationship between shear wave velocity (V_s) and fundamental frequency according to the equation $h \approx V_s/4 \cdot f_0$ [24]. This was done

because the layer thickness and shear wave velocity are the most influential variables for the theoretical transfer function [31,32].

Table 1 The thickness values for the initial model at different fundamental frequencies.

Fundamental frequency	Thickness
< 0.3 Hz	350 m
0.3 - 0.5 Hz	300 m
0.5 - 0.7 Hz	250 m
0.7 - 0.9 Hz	200 m
0.9 - 1.0 Hz	150 m
1.0 - 3.0 Hz	100 m
> 3.0 Hz	50 m

We set the inversion process to search from the initial model parameters for Poisson ratios between 0.25 to 0.5, shear wave velocity between 100 to 700 m/s, and mass density between 1,000 - 3,000 kg/m^3. We allow the inversion to minimize the misfit function with 400 iterations to get the best-fitting model to the observed shear wave velocity structure data. For example, **Figure 5** shows the HVSR inversion result of survey point 24 with a fundamental frequency of 0.3 Hz that provides a good fit between observed and inverted HVSR after 400 iterations, the misfit error converges from 0.078 to 0.004 by obtaining a subsurface profile down to 300 m.

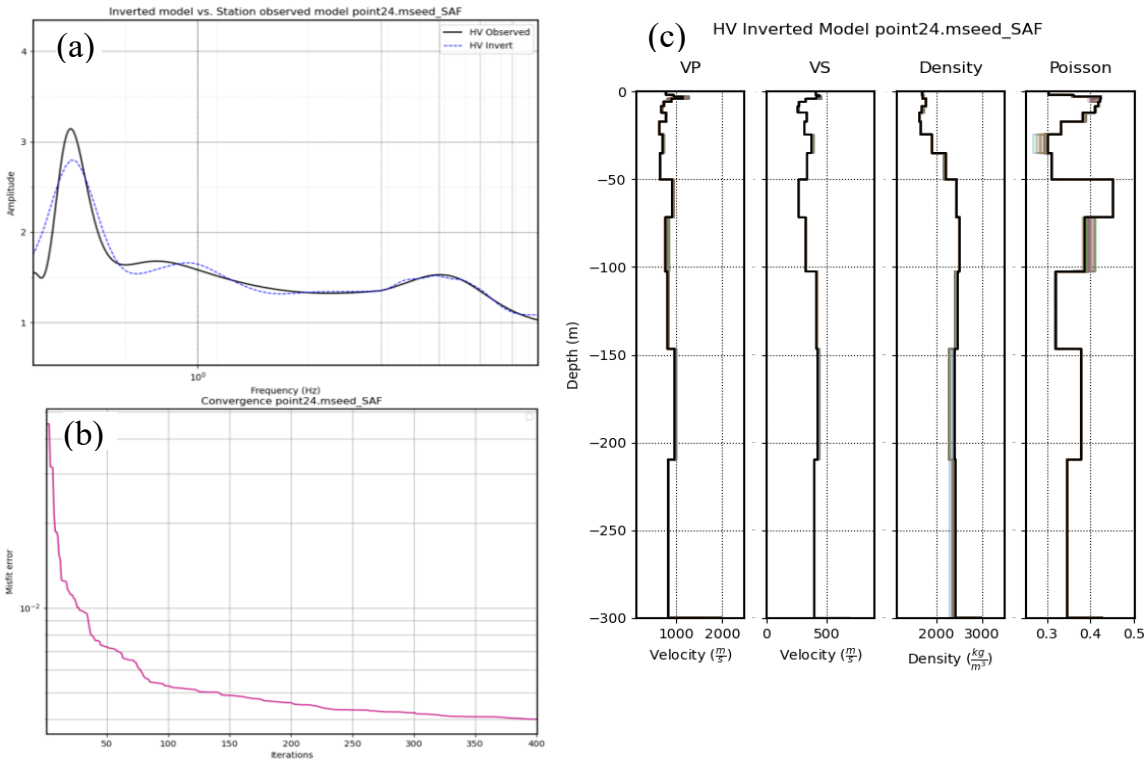

Figure 5 HVSR inversion results for velocity profiles of the survey point 24 in San Kamphaeng District. (a) Comparison between the observed HVSR curve and the HVSR inverted model. (b) Convergence of model misfit. (c) The subsurface profile from the HVSR inverted model of the P-wave velocity, shear wave velocity, density, and Poisson's ratio.

Results and discussion

Earthquake ground motion can cause potential damage or resonance if the building fundamental frequency is close to the soil fundamental frequency. The dynamic characteristics of soil depend on frequency, amplitude, and duration of vibrations. Hence, it is important to generate a seismic microzonation map for the Chiang Mai basin, according to the HVSR curve frequency-amplitude.

Map of fundamental frequency and amplification factor

Our fundamental frequency map of the Chiang Mai basin is shown in **Figure 6**. It was generated using the well-defined peak in the HVSR curve results. Approximately 70 % of all survey points met reliability and clear H/V peak criteria, and those results were gridded using adjustable tension continuous curvature splines (GMT surface interpolation).

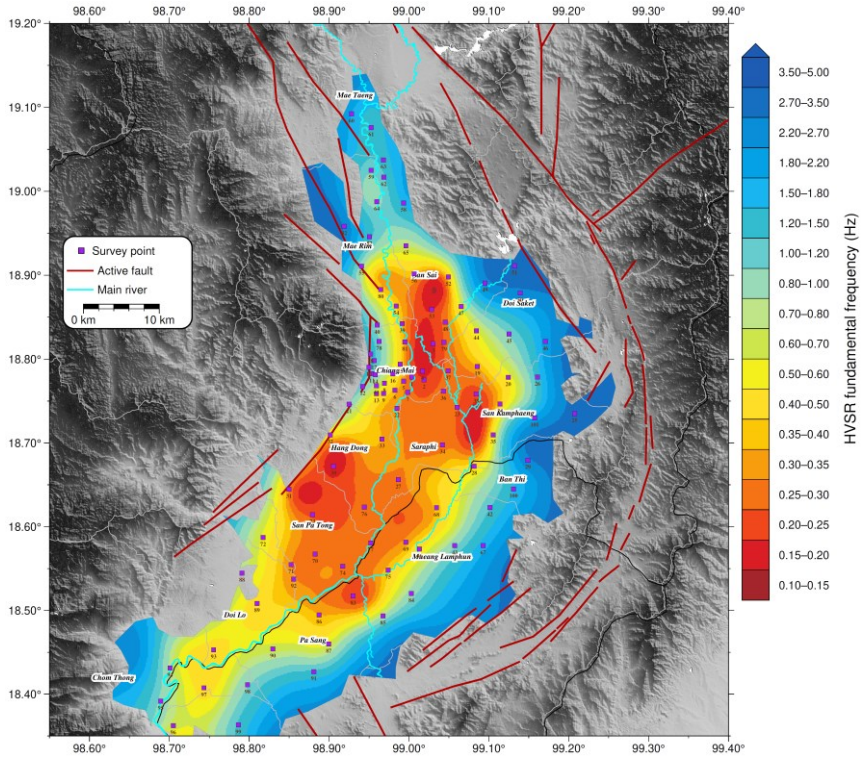

Figure 6 Map of the fundamental resonance frequency of sediment deposits of the Chiang Mai basin, Thailand derived from HVSR curves. The topography around the basin including active fault (red line) and all survey points (purple square) are shown.

We found very low fundamental frequencies ranging from 0.15 - 0.4 Hz in the middle of the Chiang Mai basin, indented to the west of the basin. This means that there is a thick layer of sediment in the middle of the basin, with increasing fundamental frequency approaching the edge of the basin. This is in close proximity to the location of the basin depocenter interpreted from gravity data in the Chiang Mai basin area [2,4]. The very low frequency resonance (0.2 - 0.4 Hz) is intended for areas with a bedrock depth of 500 - 1,800 m [33]. An interesting result is that the western edge of the basin shows distinctly low fundamental frequencies (~0.5 Hz) adjacent to the highland. This is related to the observed very rapid Bouguer gravity anomaly increase toward the Doi Suthep mountain [4], indicating that the western margin of the Chiang Mai basin has a steep slope. On the eastern side of the basin, the frequency gradually increases from the

central basin to the mountain range, representing the low-angle west-dipping Carboniferous basement on the eastern edge of the Chiang Mai basin [5].

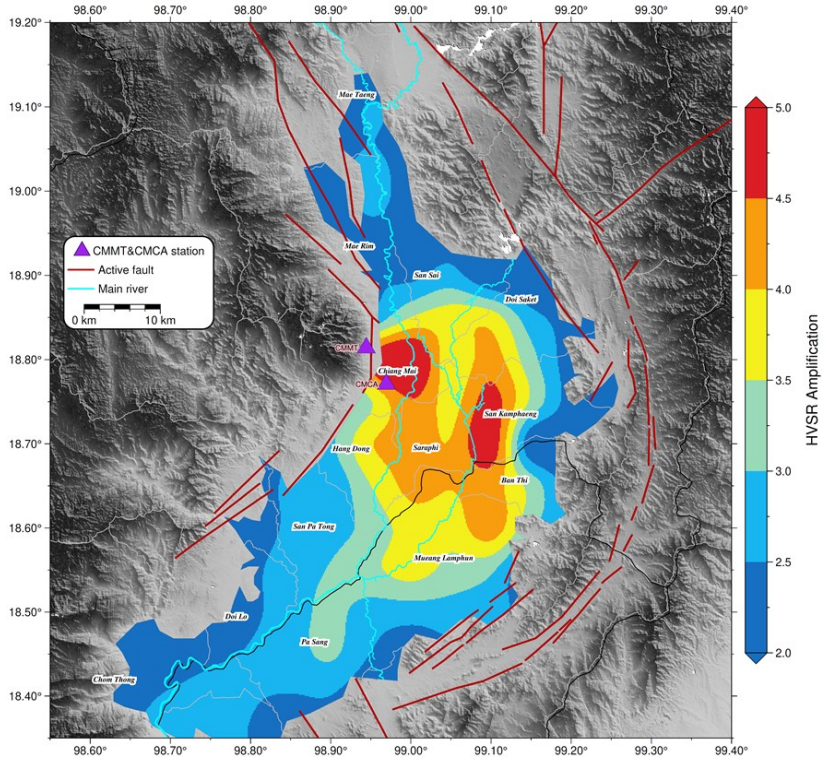

Figure 7 Map of ground motion amplification (A_0) of a sediment deposit of the Chiang Mai basin, Thailand derived from HVSR curves for frequencies less than 2 Hz.

The ground motion amplification (A_0) of the HVSR curves is affected by the density contrast between a basal hard layer and the overlying soft sediment layer. The amplification of ground motion in Chiang Mai basin from the HVSR amplitude ratio for frequencies less than 2 Hz (displayed in **Figure 7**) shows that the amplification factor ranges between 3 - 5 times in the middle of the basin along the Ping River and the Kuang River. This is especially the case in the Mueang Chiang Mai and San Kamphaeng districts with the highest amplification factor of about 5 times.

We also analyzed HVSR using earthquake waveform data from the 5 May 2014 ML6.3 Mae Lao, Thailand earthquake, (the largest earthquake in modern Thai history), and the 21 July 2022 ML6.4 Keng Tung, Myanmar earthquake. For both of these earthquake events, shaking was reported by many residents in Chiang Mai [34]. We use waveforms observed at the CMMT station located on rock (Doi Suthep) and the CMCA station located in the basin (Chiang Mai Airport) (both operated by the Thai Meteorological Department (TMD) [35]). The station locations are shown in **Figure 7**, We compare these results to the resulting HVSR curves between rock and soil sites. The distance from the Mae Lao, Thailand, and the Keng Tung, Myanmar earthquakes to these seismic stations is about 130 km and 290 km respectively. The average HVSR curves for rock and basin sites are shown in **Figure 8(a)**. The CMMT station has a flat HVSR curve with no amplification, consistent with it being a hard rock site suitable as a reference site, while the amplification of the HVSR curve of the CMCA station from 2 earthquake events shows ground shaking amplification up to 4 - 4.5 times at a resonance frequency of about 0.4 - 0.5 Hz, which corresponds to the HVSR fundamental resonance frequency and ground motion amplification results we obtained from microtremor measurement at the Chiang Mai airport area and shown in **Figures 6** and **7**. The second peak (high frequency peak of ~5 - ~6 Hz) was found to be significantly related to the shallow impedance contrast between soft clay and gravel [36]. **Figure 8(b)** shows the raw acceleration records of the 21 July 2022 ML6.4, Keng Tung, Myanmar earthquake, and we observe that the CMCA station has a peak ground

acceleration (PGA) of 0.0192 m/s^2, which is approximately 4.5 times higher than the CMMT station (0.0043 m/s^2) which is related to the amplifying effect seen in the HVSR curve.

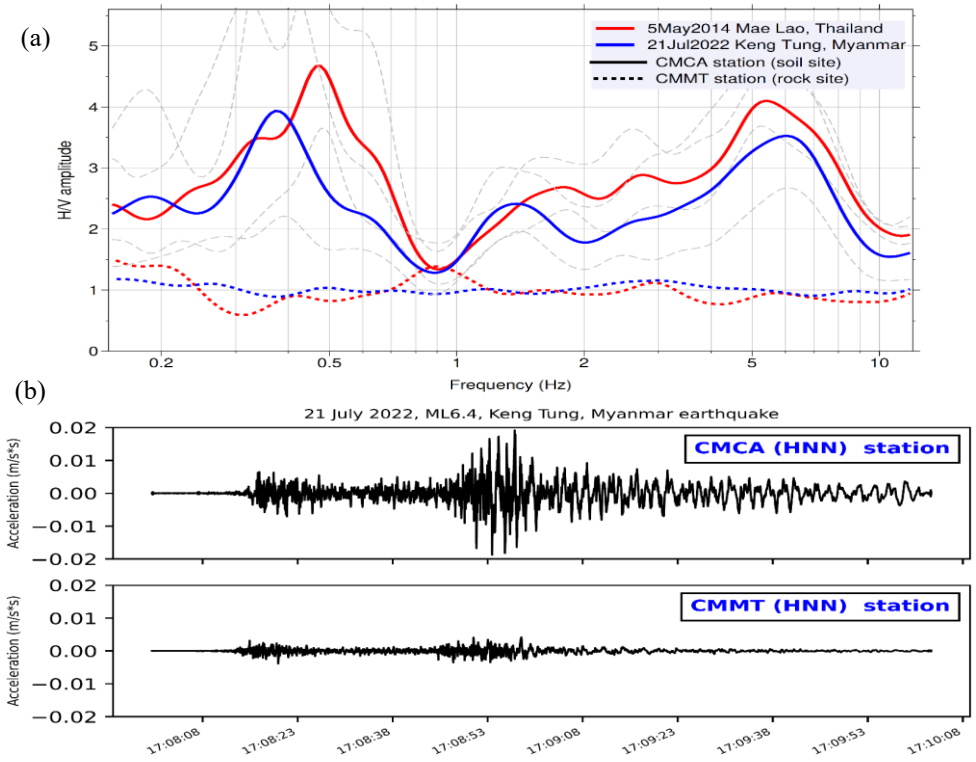

Figure 8 (a) average HVSR curve of the CMCA station on the soil site (solid line) and CMMT station on the rock site (dotted line) derived from the 5 May 2014 ML6.3 Mae Lao, Thailand earthquake (red) and 21 July 2022 ML6.4 Keng Tung, Myanmar earthquake (blue). The dashed gray line indicates the minimum and maximum HVSR curve of the CMCA station of both events. (b) Raw acceleration records of 21 July 2022 ML6.4, Keng Tung, Myanmar earthquake comparing the peak ground acceleration (PGA) of basin site (CMCA) and rock site (CMMT), with its epicenter around 290 km to both stations.

Vs30 and NEHRP site classification

The average shear wave velocity to 30 m depth (Vs30) for each survey point is determined from inversion of the ambient noise HVSR curve. The map of Vs30 across the Chiang Mai basin is shown in **Figure 9**. We found that the Vs30 was significantly lower in the middle of the basin, in Muang Chiangmai, Saraphi, the south part of Sansai district, and the north part of Lumphun province, where the Vs30 value ranged from 150 to 250 m/s. This corresponds to a geologic soil profile where the soils are mostly soft sediments from alluvial plains and floodplain deposits. These Vs30 results agree with the results from MASW method in [6] and the inversion using the Centerless Circular Array survey method in [9]. We classify soil types according to the National Earthquake Hazard Reduction Program (NEHRP) classification, using the Vs30 value. The soil classification map is shown in **Figure 10**. The lowest Vs30 values, which are in the north part of the Saraphi district and are lower than 180 m/s, place this site as class E (soft soil). The class D soil (stiff soil) area corresponds to the alluvium sediments (Qa) shown in the geologic map (**Figure 2**). The class C soil (very dense soil) area matches the tertiary and quaternary basin sediments (Qt) on the geologic map and are consistent with the results from SPAC method in [8]. It can be seen that most Qt sediment is located on the eastern edge of the basin.

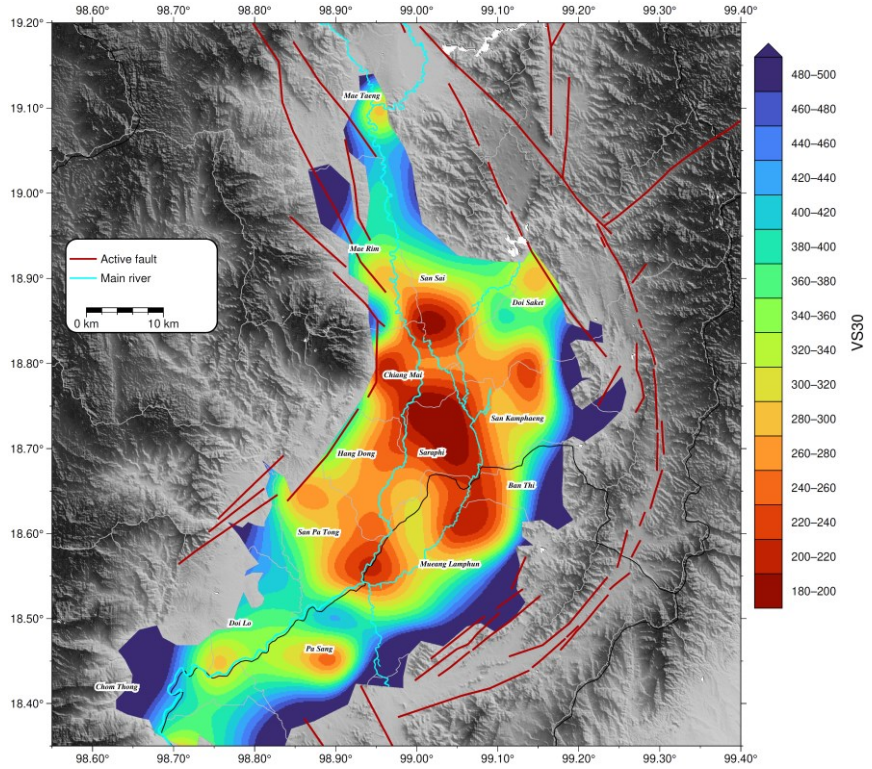

Figure 9 The spatial variability of the average shear wave velocity Vs30 map of Chiang Mai basin, Thailand derived from HVSR inversion.

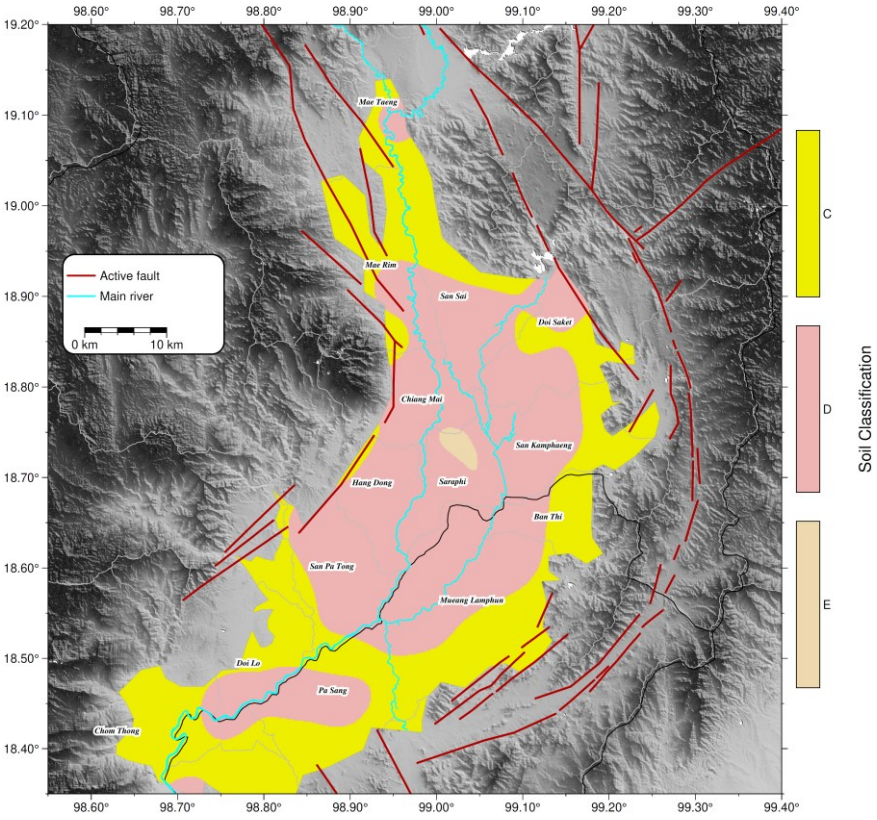

Figure 10 Site Classification map of Chiang Mai basin by NEHRP classification.

Conclusions

The Chiang Mai basin and the major part of Chiang Mai City are situated on unconsolidated sediments derived from the Ping River and Kuang River. These sediments have a low fundamental frequency, which ranges from 0.15 - 0.4 Hz in the middle and extends to the west of the Chiang Mai basin, which is proximal to the location of the basin depocenter. The western edge of the basin has low frequencies (~0.5 Hz) adjacent to the highlands, indicating a steep slope to the western margin of the Chiang Mai basin. On the eastern side of the basin, the fundamental frequency gradually increases from the central basin to the mountain range. This likely represents a low-angle dipping basement contact of the eastern edge of the Chiang Mai basin. Most of the Chiang Mai basin area is classified as site D soil (stiff soil) using the Vs30 NEHRP classification. This indicates that the Chiang Mai basin is at high risk from seismic amplification that amplifies ground motion between 3 - 5 times in the middle of the basin, especially in the cities of Chiang Mai and San Kamphaeng.

Acknowledgements

This research is funded by Thailand Science Research and Innovation (TSRI) (Project No. 159210) and supported by the Thai Meteorological Department. We would like to acknowledge the survey teams, Ms. Naruemon Teerakung, Ms. Wanatchaporn Rungjaeng, and Ms. Nuttarinee Boonchu from the Earthquake Observation Division, of the Thai Meteorological Department.

References

[1] P Pananont and P Pornsopin. A possible hidden fault in Chiang Mai, Northern Thailand from microseismicity. *Eur. Assoc. Geoscientists Eng.* 2020; **2020**, 1-4.

[2] C Morley, P Charusiri and I Watkinson. *Structural geology of Thailand during the Cenozoic Modern tectonic setting of Thailand*. ResearchGate, Berlin, Germany, 2011.

[3] North Geological Maps by Province, Available at: https://gisportal.dmr.go.th/portal/apps/MapSeries/index.html?appid=927a0f2c42f44c40ab6cb03109682ebf, accessed 24 May 2023.

[4] K Wattananikorn, JA Beshir and A Nochaiwong. Gravity interpretation of Chiang Mai Basin, northern Thailand: Concentrating on Ban Thung Sieo area. *J. Southeast Asian Earth Sci.* 1995; **12**, 53-64.

[5] N Mankhemthong, C Phanratana and S Udphuay. Lithologic modeling using VES method for subsurface structure delineation with geological constraints, eastern margin of Chiang Mai Basin and southwestern margin of Mae On Depression, San Kamphaeng District, Chiang Mai Province, northern Thailand. *Geosci. J.* 2020; **25**, 479-94.

[6] T Thitimakorn. Development of a NEHRP site classification map of Chiang Mai city, Thailand, based on shear-wave velocity using the MASW technique. *J. Geophys. Eng.* 2013; **10**, 045007.

[7] T Thitimakorn and T Raenak. NEHRP site classification and preliminary soil amplification maps of Lamphun City, Northern Thailand. *Open Geosci.* 2016; **8**, 538-47.

[8] P Thamarux, M Matsuoka, N Poovarodom and J Iwahashi. VS30 seismic microzoning based on a geomorphology map: Experimental case study of Chiang Mai, Chiang Rai, and Lamphun, Thailand. *ISPRS Int. J. Geo Inform.* 2019; **8**, 309.

[9] N Poovarodom, A Jirasakjamroonsri and P Warnitchai. Site characteristics of Chiang Mai, Thailand from array microtremor observations. *In*: Proceedings of the 8th Asia Conference on Earthquake Engineering, Taipei, Taiwan. 2022.

[10] I Cho, T Tada and Y Shinozaki. Centerless circular array method: Inferring phase velocities of Rayleigh waves in broad wavelength ranges using microtremor records. *J. Geophys. Res.* 2006; **111**, B09315.

[11] Y Nakamura. A method for dynamic characteristics estimation of subsurface using microtremor on the ground surface. *Jpn. Natl. Railways* 1989; **30**, 25-33.

[12] LS Schleicher and TL Pratt. Characterizing fundamental resonance peaks on flat-lying sediments using multiple spectral ratio methods: An example from the atlantic coastal plain, Eastern United States. *Bull. Seismol. Soc. Am.* 2021; **111**, 1824-48.

[13] S Khan, M Waseem, S Khalid, DP Kontoni, M Ahmad and S Keawsawasvong. Fuzzy clustering analysis of HVSR data for seismic microzonation at Lahore city. *Shock Vib.* 2022; **2022**, 3109609.

[14] A Krylov, M Kulikov, S Kovachev, I Medvedev, L Lobkovsky and I Semiletov. Peculiarities of the HVSR method application to seismic records obtained by Ocean-Bottom seismographs in the arctic. *Appl. Sci.* 2022; **12**, 9576.
[15] M Yazdi, R Motamed and JG Anderson. A new set of automated methodologies for estimating site fundamental frequency and its uncertainty using Horizontal-to-Vertical spectral ratio curves. *Seismol. Res. Lett.* 2022; **93**, 1721-36.
[16] O Alonso, D Bernal, J Torrijo and J Garzón-Roca. A comparative analysis for defining the sliding surface and internal structure in an active landslide using the HVSR passive geophysical technique in Pujilí (Cotopaxi), ecuador. *Land* 2023; **12**, 961.
[17] L Ávila-Barrientos, L Yegres and HF Estrella. Characterization of landslides in federal highway 1D, Baja California, Mexico, using seismic noise records and the HVSR method. *Nat*. *Hazards* 2023; **118**, 28806.
[18] F Ghione, A Köhler, A Dichiarante, I Aarnes and V Oye. Vs30 and depth to bedrock estimates from integrating HVSR measurements and geology-slope approach in the Oslo area, Norway. *Front. Earth Sci.* 2023; **11**, 1242679.
[19] Y Zhang, X Wei, Y Li, S Jeong and T Ku. Sediment thickness and average Vs prediction using HVSR of ambient seismic noise: Case studies in Singapore. *Bull. Eng. Geol. Environ.* 2023; **82**, 195.
[20] A Rigo, E Sokos, V Lefils and P Briole. Seasonal variations in amplitudes and resonance frequencies of the HVSR amplification peaks linked to groundwater. *Geophys. J. Int.* 2021; **226**, 1-13.
[21] S Koley. Future perspectives and mitigation strategies towards groundwater arsenic contamination in West Bengal, India. *Environ. Qual. Manag.* 2022; **31**, 75-97
[22] BSS Council. NEHRP recommended provisions for seismic regulations for new buildings and other structures.FEMA, Washington DC, 1997.
[23] K Konno and T Ohmachi. Ground-motion characteristics estimated from spectral ratio between horizontal and vertical components of microtremor. *Bull. Seismol. Soc. Am.* 1998; **88**, 228-41.
[24] PY Bard, C Acerra, G Aguacil, A Anastasiadis, K Atakan, R Azzara, R Basili, E Bertrand, B Bettig, F Blarel, S Bonnefoy-Claudet, B Paola, A Borges, M Sørensen, L Bourjot, H Cadet, F Cara, A Caserta, JL Chatelain and S Zacharopoulos. Guidelines for the implementation of the H/V spectral ratio technique on ambient vibrations measurements, processing and interpretation. *Bull. Earthquake Eng.* 2008; **6**, 1-2.
[25] J Rodrigues and R Brincker. Application of the random decrement technique in operational modal analysis. *In*: Proceedings of the 1st International Operational Modal Analysis Conference, Copenhagen, Denmark. 2005.
[26] J Piña-Flores, M Perton, A García-Jerez, E Carmona, F Luzon, JM Villegas and F Sánchez-Sesma. The inversion of spectral ratio H/V in a layered system using the Diffuse Field Assumption (DFA). *Geophys. J. Int.* 2016; **208**, 577-88.
[27] A García-Jerez, J Piña-Flores, F Sánchez-Sesma, F Luzon and M Perton. A computer code for forward calculation and inversion of the H/V spectral ratio under the diffuse field assumption. *Comput. Geosci.* 2016; **97**, 67-78.
[28] F J Sánchez-Sesma, M Rodríguez, U Iturrarán-Viveros, F Luzón, M Campillo, L Margerin, A García-Jerez, M Suarez, M A Santoyo and A Rodríguez-Castellanos. A theory for microtremor H/V spectral ratio: application for a layered medium. *Geophys. J. Int.* 2011; **186**, 221-5.
[29] R Manzo, L Nardone, G Gaudiosi, C Martino, D Galluzzo, F Bianco and RD Maio. A first 3-D shear wave velocity model of the Ischia Island (Italy) by HVSR inversion. *Geophys. J. Int.* 2022; **230**, 2056-72.
[30] AH Farazi, MS Hossain, Y Ito, J Piña-Flores, ASMM Kamal and MZ Rahman. Shear wave velocity estimation in the Bengal Basin, Bangladesh by HVSR analysis: Implications for engineering bedrock depth. *J. Appl. Geophys.* 2023; **211**, 104967.
[31] S Foti, C Comina, D Boiero and L Socco. Non-uniqueness in surface-wave inversion and consequences on seismic site response analyses. *Soil Dynam. Earthquake Eng.* 2009; **29**, 982-93.
[32] S Molnar, SE Dosso and JF Cassidy. Bayesian inversion of microtremor array dispersion data in southwestern British Columbia. *Geophys. J. Int.* 2010; **183**, 923-40.
[33] S Marcucci, G Milana, S Hailemikael, G Carlucci, F Cara, G Di Giulio and M Vassallo. The deep bedrock in Rome, Italy: A new constraint based on passive seismic data analysis. *Pure Appl. Geophys.* 2019; **176**, 2395-410.
[34] Earthquake Observation Division; Thai Meteorological Department, Available at: https://earthquake.tmd.go.th/inside-info.html?earthquake=9176, accessed 31 August 2023.

[35] P Pornsopin, P Pananont, KP Furlong and E Sandvol. Sensor orientation of the TMD seismic network (Thailand) from P-wave particle motions. *Geosci. Lett.* 2023; **10**, 24.
[36] A Macau, B Benjumea, A Gabàs, S Figueras and M Vilà. The effect of shallow quaternary deposits on the Shape of the H/V spectral ratio. *Surv. Geophys.* 2015; **36**, 185-208.